Journal Pre-proofs

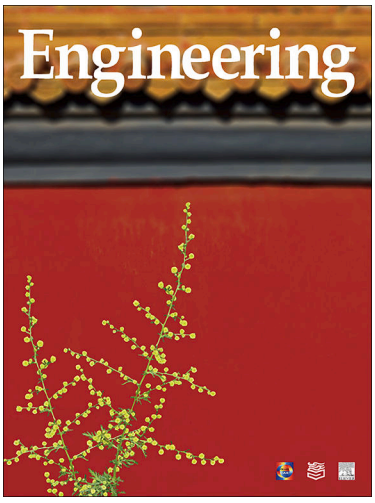

Article

Pilot-Scale Solar Powered Two-Stage Humidification–Dehumidification Desalination With Freshwater Absorption and Fine-Grained Heat Recovery

Shen Liang, Cancan Zhang, Yuting Wu, Yanjie Zheng, Yasong Sun, Yifan Wang, Xinglong Ma

PII: S2095-8099(26)00453-4
DOI: https://doi.org/10.1016/j.eng.2026.08.013
Reference: ENG 2437

To appear in: *Engineering*

Received Date: 11 December 2025
Revised Date: 21 July 2026
Accepted Date: 6 August 2026

Please cite this article as: S. Liang, C. Zhang, Y. Wu, Y. Zheng, Y. Sun, Y. Wang, X. Ma, Pilot-Scale Solar Powered Two-Stage Humidification–Dehumidification Desalination With Freshwater Absorption and Fine-Grained Heat Recovery, *Engineering* (2026), doi: https://doi.org/10.1016/j.eng.2026.08.013

This is a PDF of an article that has undergone enhancements after acceptance, such as the addition of a cover page and metadata, and formatting for readability. This version will undergo additional copyediting, typesetting and review before it is published in its final form. As such, this version is no longer the Accepted Manuscript, but it is not yet the definitive Version of Record; we are providing this early version to give early visibility of the article. Please note that Elsevier's sharing policy for the Published Journal Article applies to this version, see: https://www.elsevier.com/about/policies-and-standards/sharing#4-published-journal-article. Please also note that, during the production process, errors may be discovered which could affect the content, and all legal disclaimers that apply to the journal pertain.

© 2026 THE AUTHORS. Published by Elsevier LTD on behalf of Chinese Academy of Engineering and Higher Education Press Limited Company

Journal Pre-proofs

Environmental Frontiers for Water–Energy Nexus—Article

Pilot-Scale Solar Powered Two-Stage Humidification–Dehumidification Desalination With Freshwater Absorption and Fine-Grained Heat Recovery

Shen Liang[a], Cancan Zhang[a], Yuting Wu[a], Yanjie Zheng[b], Yasong Sun[c], Yifan Wang[d,*], Xinglong Ma[e,*]

[a]*College of New Energy, Beijing University of Technology, Beijing 100124, China*

[b]*School of Mechanical Engineering, Beijing Institute of Technology, Beijing 100081, China*

[c]*Shaanxi Key Laboratory of New Transportation Energy and Automotive Energy Saving, School of Power and Electric Engineering, Chang'an University, Xi'an 710018, China*

[d]*School of Energy and Power Engineering, Xi'an Jiaotong University, Xi'an 710049, China*

[e]*School of Environment, Nanjing Normal University, Nanjing, 210023, China*

Corresponding authors.
E-mail addresses: 75061@njnu.edu.cn (X. Ma), leibeleon@163.com (Y. Wang).

Abstract

Humidification–dehumidification (HDH) desalination is attractive for decentralized small- and medium-scale freshwater production because it operates at atmospheric pressure and can be driven by solar thermal energy and other low-temperature heat sources. However, conventional HDH systems are still limited by coarse and temperature-mismatched internal heat recovery, which underutilizes recoverable latent heat and brine sensible heat from condensation for subsequent evaporation demand. This leads to low gained output ratios (GORs), bulky heat and mass transfer components, and high thermal consumption. To address these limitations, this paper proposes a fine-grained heat recovery strategy by routing feed seawater through multiple heat recovery stages and using dual condensation to recover latent heat from high-temperature humid air. A pilot-scale two-stage HDH desalination system powered by a 120 m^2 solar vacuum tube collector array was designed and tested, with vertically stacked high- and low-temperature stages for compactness. Experiments across spray temperatures of 62–80 ℃, followed by a full-day test under fluctuating solar irradiance, were conducted to evaluate freshwater production and GOR. At a spray temperature of 80 ℃, the system achieved a freshwater production rate of 97.2 kg • h^{-1} and a GOR of 1.78. The reheating process increased freshwater production from 88.2 to 97.2 kg • h^{-1} and improved the GOR from 1.71 to 1.78. Under fluctuating solar conditions, the daily freshwater production reached 860 kg, corresponding to 7.17 kg • m^{-2} • day^{-1} on the basis of the collector aperture area. These findings demonstrate the effectiveness of the fine-grained heat recovery strategy and support the advancement of HDH desalination toward higher efficiency and lower thermal consumption.

Keywords: Humidification and dehumidification (HDH); Fine-grained heat recovery; Solar thermal desalination; Stacked structure; Freshwater absorption.

1. Introduction

Freshwater scarcity is a persistent global challenge intensified by population growth, industrialization, and uneven water resource distribution [1]. Desalination provides a key pathway for freshwater augmentation and sustainable water security [2]. Reverse osmosis (RO) [3], multi-stage flash (MSF) [4], mechanical vapor compression (MVC) [5], and multiple-effect distillation (MED) [6] have been widely deployed in water scarce regions [7], especially in the Middle East [8]. However, their reliance on high-grade energy supply, centralized infrastructure, and complex operation limits their suitability for decentralized small- and medium-scale applications [9]. Membrane distillation (MD) has also received increasing attention as an emerging thermally driven membrane process [10]. However, it remains mainly at the laboratory or pilot-scale [11], with large-scale applications constrained by membrane wetting, fouling, scaling, and heat recovery limitations [12].

In contrast, humidification–dehumidification (HDH) desalination has emerged as a promising thermal desalination technology for distributed small-scale freshwater production [13]. The HDH desalination process mimics the natural water cycle and can handle a wide range of salinity levels [14], from brackish water to seawater [15]. The HDH system operates at atmospheric pressure and can be made of nonmetallic corrosion-resistant materials [16]. Importantly, the HDH desalination process typically operates at temperatures of approximately 45 to 90 ℃, which allows it to be effectively driven by solar thermal energy [17] or low-temperature waste heat [18]. As a representative waste heat-driven HDH configuration, Aboelmaaref et al. [19] utilized the waste heat rejected from a silica gel-based adsorption desalination cycle to preheat saline water and drive the subsequent HDH desalination process.

A typical HDH desalination system comprises three essential components; a humidifier, a dehumidifier, and a heating

source [20]. The heating source elevates the temperature of either the air or the feed seawater before it enters the humidifier, whe[illegible]. In this context, HDH desalination systems can be categorized according to their air and water circulation configurations into open-air open-water (OAOW), open-air closed-water (OACW), closed-air open-water (CAOW), and closed-air closed-water (CACW) systems [22]. In addition to air and water circulation configurations, HDH systems are commonly classified by structural staging into single- and multi-stage configurations [23], depending on whether one or multiple humidifier–dehumidifier pairs are used to enable cascaded reuse of condensation latent heat [24]. A single-stage HDH system consists of one humidifier and dehumidifier pair, in which porous packing materials are used to increase the air–water contact area and enhance heat and mass transfer [25]. Such packing materials are generally required to provide a large specific surface area, low pressure drop [26], good corrosion resistance, and acceptable cost [27].

Single-stage HDH systems have simple configurations but typically exhibit low gained output ratios (GORs), primarily because the latent heat of condensation and sensible heat of brine are insufficiently recovered within the humidification–dehumidification loop [28]. During humidification, heat supplied to the air–water contact process drives seawater evaporation and consumes substantial latent heat. During dehumidification, vapor condensation releases latent heat, but only a limited fraction is effectively reused for subsequent evaporation. Consequently, typical single-stage HDH desalination systems often present GORs in the range of 0.3–0.8 [29]. For example, Liang et al. [30] developed a single-stage HDH desalination unit with an internal air duct and freshwater absorption dehumidification for an onboard potable water supply. At a heat source temperature of 90 ℃, the system produced 19.6 $kg \cdot h^{-1}$ of freshwater with a GOR of 0.53.

To address the limited heat recovery of single-stage HDH systems, we developed multi-stage configurations to enable cascaded recovery and the reuse of condensation latent heat for evaporation in subsequent stages [31]. Such staged heat reuse allows the supplied thermal energy to participate in multiple evaporation–condensation processes, thus improving freshwater productivity and GOR compared with those of single-stage systems [32]. Zamen et al. [33] experimentally evaluated a two-stage HDH system for brackish water desalination and reported a 20% increase in freshwater yield compared with that of a single-stage system. Zhao et al. [34] reported a four-stage solar HDH desalination system that achieved a freshwater production rate of 34.1 $kg \cdot m^{-3} \cdot h^{-1}$ and a GOR of 1.4 through numerical and experimental analyses. However, the performance improvements of multi-stage HDH desalination systems often require more complex interstage heat recovery and flow distribution. This increases the pressure drop, heat loss, maldistribution risk, and equipment volume, thus limiting compact and decentralized applications [35]. To improve compactness, Yang et al. [36] developed a two-stage HDH system in which two humidification stages were thermally coupled to a shared dehumidification chamber, achieving a GOR of 0.84. However, its internal thermal management remains coarse-grained, as vapor latent heat is recovered mainly through bulk condensation rather than through a staged and temperature-matched pathway. Consequently, latent heat utilization and GOR enhancement remain constrained.

To summarize, HDH performance is limited not only by the number of stages but also by the coarse recovery and redistribution of sensible and latent heat within the humidifier and dehumidifier. In conventional HDH systems, the feed seawater in the dehumidifier recovers latent heat mainly through bulk condensation, and this coarse, single-step process prevents thermodynamic matching with downstream temperature requirements [37]. As a result, the preheated feed seawater still requires substantial external heating before entering the humidifier, or is partially discarded, leading to significant sensible heat loss. Moreover, the latent heat of water evaporation is approximately 2.3×10^6 $J \cdot kg^{-1}$, compared with only 4.2×10^3 $J \cdot kg^{-1} \cdot ℃^{-1}$ to increase the seawater temperature by 1 ℃. Thus, the latent heat of evaporation is approximately three orders of magnitude greater than the sensible heat required to heat seawater. Consequently, maintaining the evaporation temperature requires a large latent heat supply, which in conventional HDH systems is typically achieved by increasing the spray feed seawater flow rate. This, in turn, forces large volumes of heated seawater to circulate through the system and ultimately be discharged as brine, causing substantial sensible heat loss.

Therefore, this work shifts the focus from simply increasing the number of HDH stages to restructuring the internal thermal pathway. A fine-grained heat recovery strategy is proposed by routing feed seawater through multiple temperature-matched recovery nodes and introducing dual condensation of high-temperature humid air. The fine-grained heat recovery strategy enables the sensible heat of brine and the latent heat released during condensation to be more effectively recovered and redistributed for subsequent evaporation, thus strengthening interstage thermal coupling and reducing external heat demand. To implement and validate the proposed approach, a pilot-scale two-stage HDH desalination system fully driven by a 120 m^2 vacuum tube solar collector array was designed and experimentally investigated. The high and low-temperature stages were vertically stacked to improve the compactness of the HDH desalination module. Theoretical analysis and pilot-scale experiments demonstrate that this fine-grained, temperature-matched heat recovery concept provides a practical and effective route for advancing HDH desalination toward higher efficiency and lower thermal consumption.

2. Methods

2.1. Operating principle of fine-grained heat recovery

The operating principle of the pilot-scale, fully solar powered two-stage HDH desalination system is illustrated in Fig. 1. The system consists mainly of a solar vacuum tube collector array, a solar hot water tank, a photovoltaic module for an

Journal Pre-proofs

auxiliary power supply, and a vertically stacked two-stage HDH desalination unit. The solar vacuum tube collector array heats the w[illegible]er to heat the feed seawater entering the desalination unit. The electricity required by the pumps and circulation fans is supplied by the photovoltaic module. Thus, the system achieves full solar-driven operation by using solar thermal energy for heat supply and photovoltaic electricity for auxiliary power demand.

Journal Pre-proofs

The desalination module comprises a high-temperature stage and a low-temperature stage arranged in a vertical configuration to improve compactness. Each stage contains a humidifier and a dehumidifier. Corrugated packing is installed in both the humidifiers and dehumidifiers to increase the air and liquid interfacial area, thus enhancing coupled heat and mass transfer during humidification and dehumidification. The packing is uniformly wetted by liquid distributors with densely spaced 2-mm orifices, which promotes stable liquid distribution and helps reduce local dry zones and scaling-induced blockage.

Each stage operates with an independent closed air loop, in which the circulating air passes successively through the packed humidifier and dehumidifier. The circulating air enters the humidifier, where it directly contacts the sprayed seawater and is heated and humidified through coupled heat and mass transfer. The hot humid air then enters the dehumidifier, where it is cooled by recirculating freshwater sprayed over the corrugated packing, thus promoting vapor condensation and freshwater production. This direct contact condensation process is referred to here as freshwater absorption dehumidification, which provides a large gas–liquid contact area while separating the saline feedwater from the freshwater loop.

The fine-grained heat recovery strategy enhances internal heat recovery by recovering sensible and latent heat through temperature matched steps rather than through conventional single-step bulk heat recovery. The feed seawater is preheated by recovering brine sensible heat in the low-temperature humidifier and condensation latent heat in the low- and high-temperature dehumidifiers. After it is heated by the solar hot water tank, the feed seawater is sprayed into the high-temperature humidifier for the first evaporation process. The unevaporated seawater leaving the high-temperature humidifier is then reheated in the vapor duct by the latent heat released from partial condensation of water vapor in the hot humid air before entering the low-temperature humidifier.

More specifically, in the first heat recovery step, the feed seawater absorbs sensible heat from the discharged brine in the low-temperature humidifier, and its temperature increases from T_1 to T_2. It then flows through the freshwater basin of the low-temperature dehumidifier, where latent heat released by vapor condensation is recovered and the feed seawater temperature further increases from T_2 to T_3. In the third heat recovery step, the feed seawater flows through the coil immersed in the freshwater basin of the high-temperature dehumidifier, where higher temperature condensation latent heat is recovered and the temperature increases from T_3 to T_4. After the three heat recovery steps, the preheated feed seawater is further heated through the plate heat exchanger connected to the solar hot water tank and then sprayed into the high-temperature humidifier.

In the high-temperature humidifier, part of the sprayed feed seawater evaporates into the circulating air, producing hot humid air, while the unevaporated seawater leaves the humidifier at T_6. Since this unevaporated seawater is cooler than hot humid air, it is routed through a reheating coil in the vapor duct, where partial vapor condensation releases heat to reheat the seawater before it enters the low-temperature humidifier. This reheating step increases the temperature of the unevaporated seawater from T_6 to T_7 by recovering latent heat released from partial vapor condensation in the duct, which also produces additional freshwater. The reheated seawater then enters the low-temperature humidifier for the second evaporation process. Overall, this fine-grained heat recovery strategy recovers brine sensible heat and condensation latent heat across different temperature levels, thus reducing external heat demand and enhancing thermal coupling between the two stages without adding an extra HDH stage.

Journal Pre-proofs

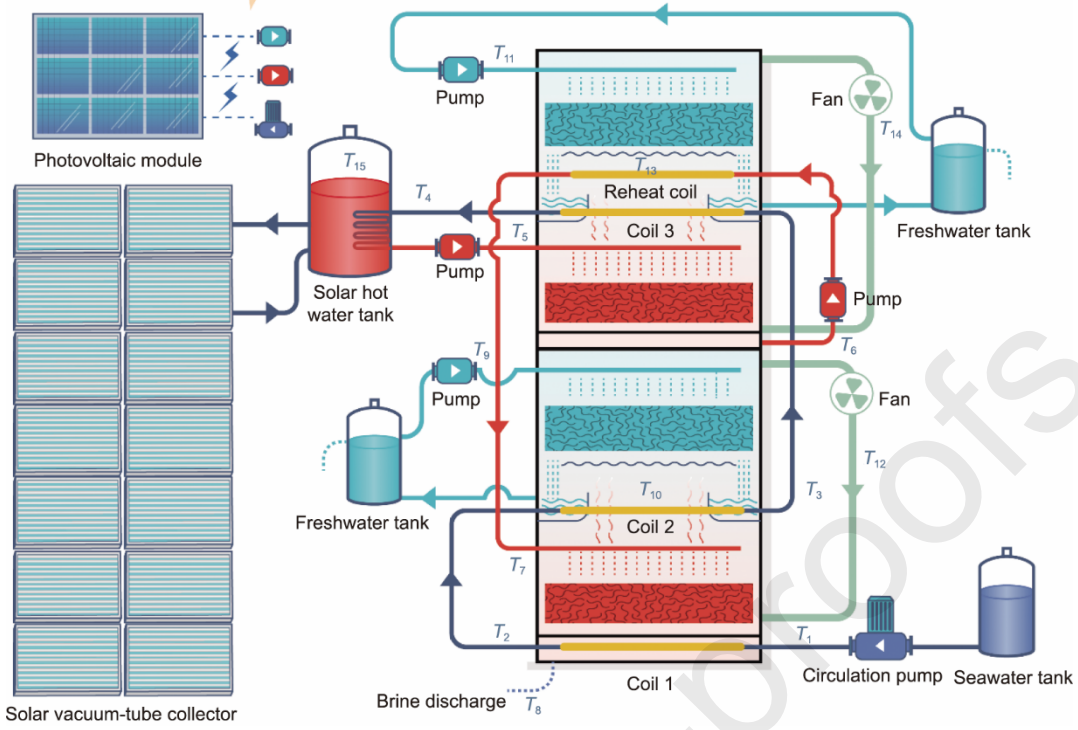

Fig. 1. Operating principle of the pilot-scale solar powered two-stage HDH desalination system

T_1: temperature of inlet feed seawater; T_2: temperature of feed seawater after the first heat recovery step; T_3: temperature of feed seawater after the second heat recovery step; T_4: temperature of feed seawater after the third heat recovery step; T_5: spray temperature of seawater in the high-temperature stage; T_6: temperature of unevaporated seawater leaving the high-temperature stage; T_7: temperature of reheated seawater entering the low-temperature humidifier; T_8: temperature of the discharged brine; T_9: spray temperature of freshwater in the low-temperature stage; T_{10}: vapor temperature in the low-temperature stage; T_{11}: spray temperature of freshwater in the high-temperature stage; T_{12}: temperature of dehumidified air in the low-temperature stage; T_{13}: vapor temperature in the high-temperature stage; T_{14}: temperature of dehumidified air in the high-temperature stage; T_{15}: temperature of the solar hot water tank.

2.2. Construction of the pilot-scale solar-driven HDH setup

To evaluate the fine-grained heat recovery strategy under realistic solar and feedwater conditions, a pilot-scale two-stage HDH desalination system fully powered by solar energy was constructed in Qinzhou, Guangxi Province (China), as shown in Fig. 2. Qinzhou is located in a coastal estuarine region subject to tidal saline intrusion from the Qinjiang estuary. Accordingly, local brackish water with a representative salinity of 1%–3.5% was used as the feedwater in the experiments. The desalination module has overall dimensions of 1.2 m × 1.2 m × 3.6 m (length × width × height), with each stage having a height of 1.8 m. The module size was determined by balancing the packed-bed height required for gas–liquid heat and mass transfer with the compactness requirement of decentralized HDH applications. The 1.8 m stage height also provides sufficient space for liquid distribution and internal heat recovery components. Polypropylene corrugated packing with a specific surface area of 300 $m^2 \cdot m^{-3}$ is installed in both the humidifier and the dehumidifier of each stage to provide a large gas–liquid contact area while maintaining a low pressure drop and good corrosion resistance under saline conditions. The heat recovery coils were fabricated from copper tubes with an outer diameter of 20 mm. Each main heat recovery coil provides a heat transfer area of 2 m^2 for preheating the feedwater. In addition, a 0.4 m^2 reheating coil was installed in the hot humid air duct for partial vapor condensation and reheating.

Feed seawater circulation is driven by two seawater feed pumps and one low pressure circulation pump, with a combined rated power of 620 W. Freshwater circulation is provided by two freshwater pumps with a combined rated power of 500 W. Each circulation fan has a rated power of 250 W. The theoretical maximum circulation flow rates are 3 $t \cdot h^{-1}$ for feed seawater, 3.5 $t \cdot h^{-1}$ for freshwater, and 400 $m^3 \cdot h^{-1}$ for circulating air. These capacities were selected to provide sufficient flexibility for matching the feed seawater, spray freshwater, and air flow rates, which are key operating parameters affecting the humidification and dehumidification processes [38, 39]. A photovoltaic module provides the electricity required to operate

the pumps and fans. Thermal energy supplied to the desalination module is delivered by a solar vacuum tube collector array with [redacted] ocal solar irradiance conditions and the heat demand of the HDH unit. A solar hot water tank was used to mitigate short term fluctuations in solar radiation and stabilize the thermal supply. A plate heat exchanger with a heat transfer area of 1.3 m^2 was used to thermally couple the desalination module with the solar collector loop. All high-temperature pipelines and exposed surfaces are thermally insulated.

Journal Pre-proofs

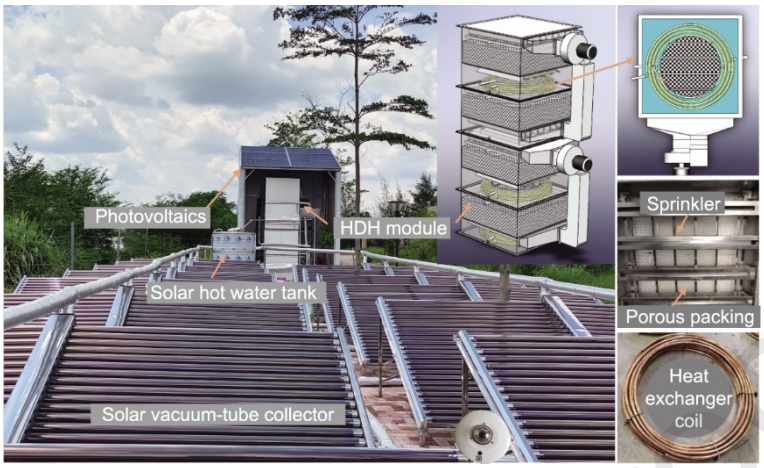

Fig. 2. Pilot-scale experimental setup of the two-stage HDH desalination and its main components

During the experiments, flow control valves and flow meters were used to regulate and measure the flow rates of the feed seawater and spray freshwater. The circulating air flow rate was measured using a hot-wire anemometer. *K*-type thermocouples were installed at the measurement points shown in Fig. 1 to monitor the temperatures of the feed seawater, spray freshwater, and humid air. The corresponding temperature signals were recorded by a multichannel temperature logger. Solar irradiance was measured using a pyranometer and recorded by a dedicated data acquisition system. Table.1 summarizes the main specifications of the pilot-scale HDH system and the measuring instruments used in the experiments.

Table. 1. Main parameters of the pilot-scale two-stage HDH system and measuring instruments

Main specifications of the pilot-scale solar-driven HDH system			Measuring instruments		
Component	Parameter	Specification	Instrumentation	Range	Accuracy
HDH module	Structure size	1.2 m × 1.2 m × 3.6 m	Temperature sensor/K type	–50–260 ℃	±0.75%
Corrugated packing	Specific surface area	300 $m^2 \cdot m^{-3}$	32-channel recorder/KSF32AOR	−200 ℃–600 ℃	±1%
Heat-recovery coils	Main/reheating coil area	2 m^2 per 0.4 m^2	Pyranometer/TRT-2	0–2000 $W \cdot m^{-2}$	±2%
Solar vacuum tube collector	Collector area	120 m^2	Hot wire anemometer/QDF-6	0.05–30 $m \cdot s^{-1}$	±5%
Maximum flow rate	Feedwater; freshwater; air	3 $t \cdot h^{-1}$; 3.5 $t \cdot h^{-1}$; 400 $m^3 \cdot h^{-1}$	Stainless steel flow meter/K24	15–150 $L \cdot min^{-1}$	±1%
Feedwater	Salinity	1%–3.5%			

3. Results and discussion

Experiments were conducted to evaluate the freshwater production performance of the pilot-scale two-stage HDH system under different high-temperature stage spray temperatures, reheating conditions, and full-day outdoor operation under fluctuating solar irradiance. In the steady-temperature tests, the solar hot water tank temperature was controlled within 70–90 ℃. Before each experiment, the solar vacuum tube collector array was operated to increase the temperature of the hot water tank (T_{15}). After the solar hot water tank reached the target temperature, the two-stage HDH desalination module was operated, with thermal energy supplied from the solar hot water tank through the plate heat exchanger. Under these conditions, the spray temperature of the feed seawater in the high-temperature stage was adjusted within the range of 62–80 ℃. This selected temperature range reflects the temperature dependent moisture-carrying capacity of air. As the saturated humidity

ratio increases nonlinearly with temperature, the evaporation driving force is limited to less than approximately 60 °C, whereas incr[Journal Pre-proofs]gher spray temperatures increase the saturated humidity ratio, operation above 80 °C is less favorable for a solar driven HDH system because of increased heat loss, scaling risk, material requirements, and solar collector demand. For each temperature condition, the feed seawater flow rate was kept constant at 2.6 $t \cdot h^{-1}$ to ensure stable spraying and adequate gas–liquid contact.

In addition, comparative tests with and without reheating of the unevaporated seawater leaving the high-temperature humidifier were performed to assess the effectiveness of the reheating process. Full-day experiments under purely solar driven operation were also carried out to evaluate the system's freshwater production performance under realistic weather conditions.

3.1 Internal temperature distributions under fine-grained heat recovery

Fig. 3 shows the variations in internal temperatures at the key measurement points of the two-stage HDH desalination module when the solar hot water tank is maintained at approximately 70 °C. A quasi-steady state is reached after approximately 20 min, indicating that the air and water circulation loops and multi-level heat recovery processes have stabilized. After stabilization, the spray feed seawater in the high-temperature stage reaches a temperature of approximately 62 °C. The dehumidified air and spray freshwater in the high-temperature dehumidifier stabilize at mean temperatures of approximately 56 and 57 °C, respectively.

In the low-temperature stage, the spray feed seawater, dehumidified air, and spray freshwater stabilize at about 57.0, 54.5, and 49.0 °C, respectively. The discharged brine remains close to 50 °C. These temperatures indicate that, under the 62 °C spray temperature condition, evaporation and condensation in both stages proceed with relatively small temperature differences for heat and mass transfer, which is consistent with HDH operation designed for internal heat recovery.

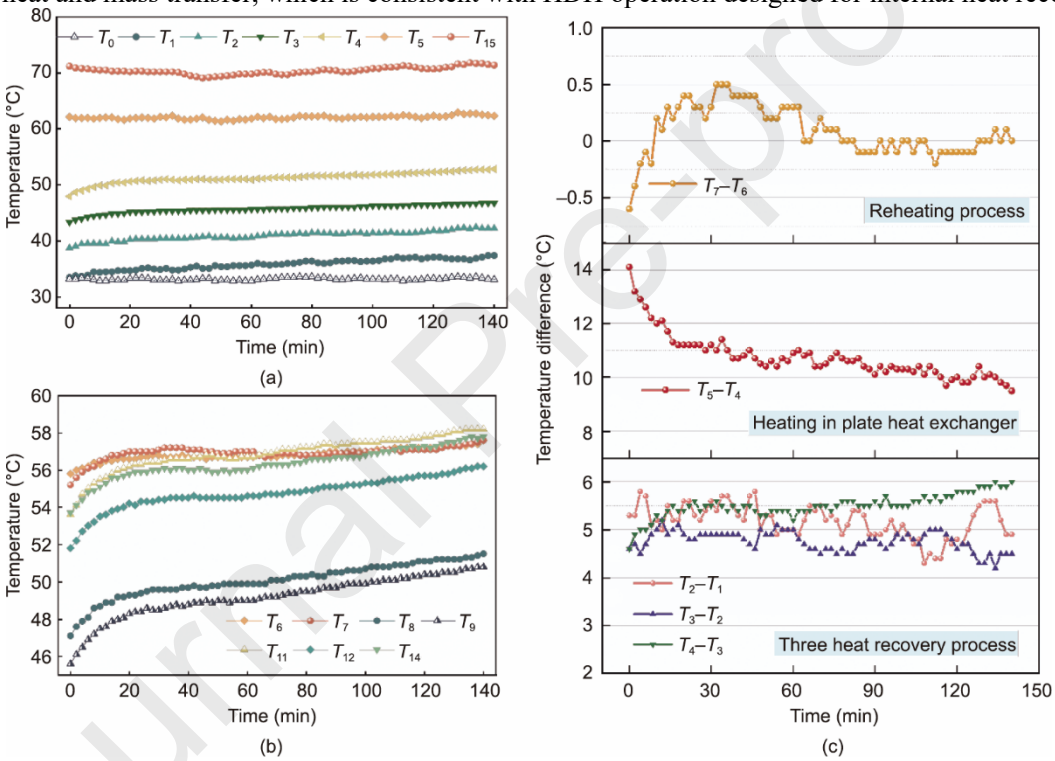

Fig. 3. Internal temperature distributions of the two-stage HDH desalination at T_5 = 62 °C; (a) Temperature evolution along the feed seawater preheating and heating pathway; (b) Temperature evolution in the high- and low-temperature HDH stages; (c) Temperature rises across the staged heat recovery, external heating, and reheating processes

To quantify the effects of internal heat recovery and reheating, in Fig. 3(c), we show the temperature increase across the three heat recovery steps, the plate heat exchanger, and the reheating process. The first, second, and third heat recovery steps result in average temperature increases of 5.2 °C (T_2–T_1), 4.8 °C (T_3–T_2), and 5.5 °C (T_4–T_3) , respectively. This finding indicates that the fine-grained heat recovery strategy effectively recovers brine sensible heat and condensation latent heat before external heating. The plate heat exchanger provides a mean temperature increase of 10.7 °C, although this temperature increase gradually decreases as the temperature difference between the hot water tank and preheated feed seawater decreases. The reheating process in the vapor duct, represented by T_7–T_6, contributes to a temperature increase of approximately 0.4 °C. This small temperature increase indicates limited heat recovery in the vapor duct under the 62 °C spray temperature condition, which is consistent with the lower vapor content and weaker condensation driving force of the hot humid air.

When the solar hot water tank reaches approximately 80 °C, the internal temperatures in the two-stage HDH module shift

to a higher level, as shown in Fig. 4. In the high-temperature stage, the spray feed seawater temperature increases to appr[illegible]s to 58.1 °C. The dehumidified air leaving the high-temperature dehumidifier stabilizes at 60.6 °C, and the spray freshwater is approximately 58.9 °C.

In the low-temperature stage, the spray seawater temperature reaches about 58.9 °C. The dehumidified air and spray freshwater stabilize at about 55.3 °C and 49.9 °C, respectively, and the discharged brine leaves at 49.2 °C. Compared with the 70 °C solar hot water tank condition, the spray seawater, dehumidified air, and spray freshwater in the low-temperature stage increase slightly, whereas the discharged brine temperature does not increase. This temperature redistribution indicates that the increased upstream thermal input is effectively conveyed to the low-temperature stage through the internal heat recovery steps and vapor duct reheating, thus enhancing the second evaporation process.

Similarly, Fig. 4(c) shows that the temperature increases across the three heat recovery steps, the plate heat exchanger, and the reheating process. The average temperature increases for the first, second, and third heat recovery steps are 4.2 , 4.0, and 7.0 °C, respectively. Compared with the 70 °C solar hot water tank condition, the third heat recovery step results in a greater temperature increase. This is attributed mainly to the higher-grade condensation heat in the high-temperature dehumidifier, where high-temperature humid air with increased moisture content transfers more latent heat to the feed seawater through the heat recovery coil. The plate heat exchanger provides a mean temperature increase of 16.0 °C. The reheating process in the vapor duct yields an average temperature increase of about 0.9 °C, suggesting that compared with the 62 °C spray temperature condition, the vapor duct has enhanced partial condensation and latent heat recovery.

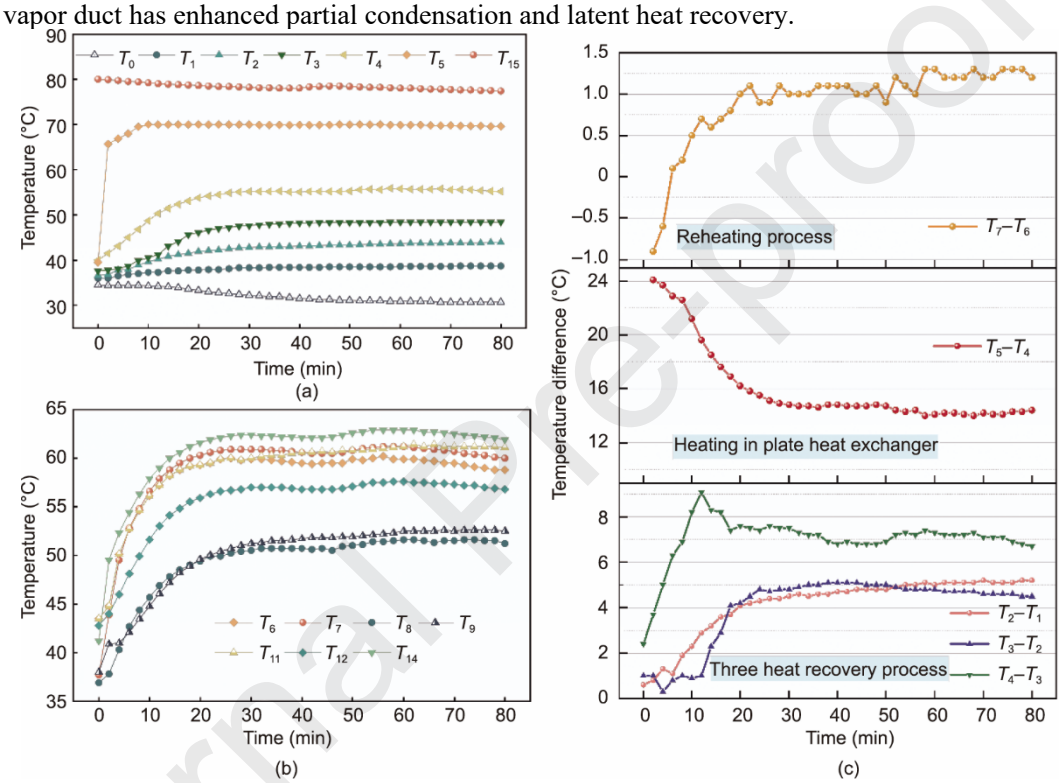

Fig. 4. Internal temperature distributions of the two-stage HDH desalination system at T_5 = 70 °C; (a) Temperature evolution along the feed seawater preheating and heating pathway; (b) Temperature evolution in the high- and low-temperature HDH stages; (c) Temperature rises across the staged heat recovery, external heating, and reheating processes

As the solar hot water tank temperature increases to approximately 85 °C, the increased thermal input further increases the internal temperature profile of the HDH module, as shown in Fig. 5. In the high-temperature stage, the spray feed seawater enters the humidifier at 75 °C. After partial evaporation and heat transfer to the circulating air, the remaining unevaporated seawater exits the humidifier at 63.8 °C. The dehumidified air leaving the high-temperature dehumidifier stabilizes at 64.6 °C, while the spray freshwater remains close to 59.3 °C. In the low-temperature stage, the spray seawater stabilized at approximately 64.5 °C, which was noticeably higher than that under the 70 and 80 °C hot water tank conditions. This increase results from the enhanced recovery of condensation heat from the higher enthalpy humid air, which increases the inlet temperature of seawater entering the low-temperature humidifier and strengthens the second evaporation process. The dehumidified air and spray freshwater reach about 61.3 and 52.9 °C, respectively. The discharged brine also exits near 52.9 °C.

The corresponding temperature increases across the three heat recovery steps, the plate heat exchanger, and the reheating process are shown in Fig. 5(c). The first, second, and third heat recovery steps yield average temperature increases of 5.4, 4.4, and 8.6 °C, respectively. After the first two recovery steps, the feed seawater has been preheated, so the low-temperature heat sources provide only limited additional temperature increases. The larger increase in the third step thus reflects better thermal

Journal Pre-proofs

matching with the high-temperature dehumidifier, allowing the condensation heat to be recovered at a higher temperature leveJournal Pre-proofs the reheating process results in a temperature increase of approximately 1.1 ℃, indicating that vapor duct reheating further strengthens the thermal coupling between the high and low-temperature stages.

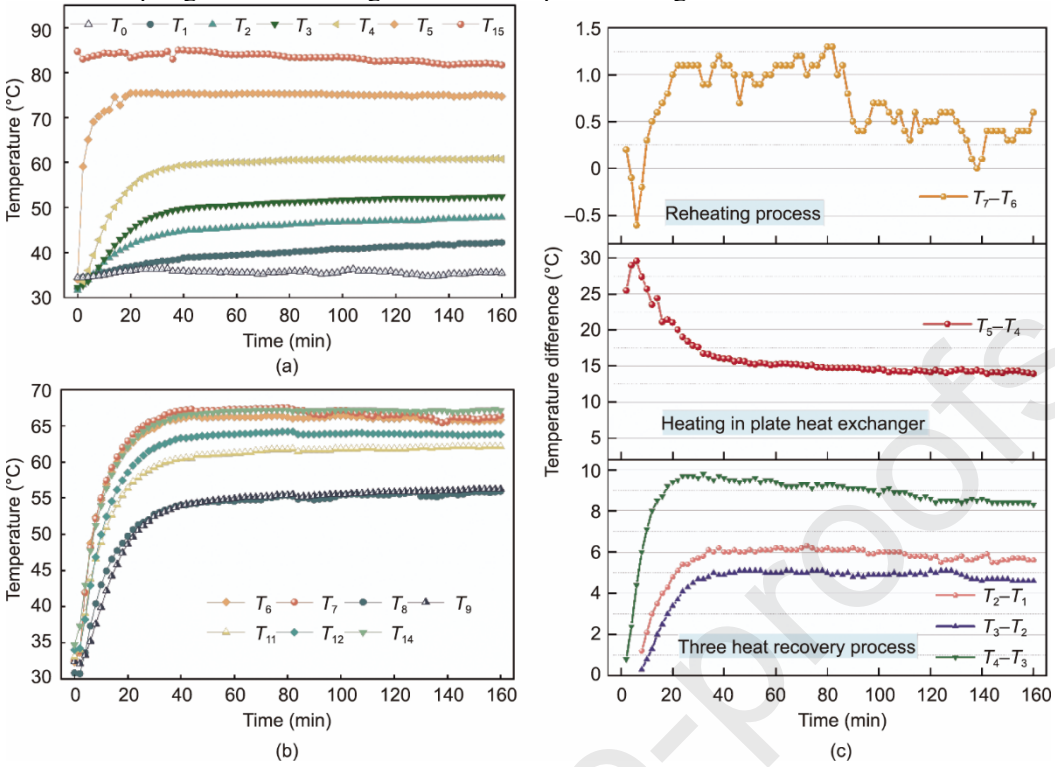

Fig. 5. Internal temperature distributions of the two-stage HDH desalination module at T_5 = 75 ℃; (a) Temperature evolution along the feed seawater preheating and heating pathway; (b) Temperature evolution in the high- and low-temperature HDH stages; (c) Temperature rises across the staged heat recovery, external heating, and reheating processes

When the solar hot water tank temperature is further increased, the high-temperature stage operates with a spray feed seawater temperature of approximately 80 ℃, as shown in Fig. 6. After partial evaporation and heat transfer to the circulating air, the remaining unevaporated seawater exits the high-temperature humidifier at about 69.3 ℃, whereas both the dehumidified air and the spray freshwater stabilize near 70 ℃. In the low-temperature stage, the temperature of the spray seawater reaches approximately 70.5 ℃, which is slightly higher than the temperature of the remaining unevaporated seawater that leaves the high-temperature humidifier, indicating that vapor duct reheating increases the seawater inlet temperature before the second evaporation process. The dehumidified air and spray freshwater stabilized at approximately 65.8 ℃ and 57.0 ℃, respectively, and the discharged brine leaves at about 56.7 ℃.

The temperature increases across the three heat recovery steps, the plate heat exchanger, and the reheating process are shown in Fig. 6(c). The first, second, and third heat recovery steps result in average temperature increases of 5.8, 5.4, and 9.9 ℃, respectively, indicating a stronger heat recovery contribution from the high-temperature dehumidifier. At a spray temperature of 80 ℃, the high-temperature dehumidifier provides the greatest internal heat recovery contribution among the tested conditions. This is because the humid air and freshwater remain near 70 ℃, which increases the temperature difference across the recovery coil and promotes the transfer of condensation heat to the feed seawater. The plate heat exchanger contributes an additional average temperature rise of 17.8 ℃. Under these conditions, the reheating process in the vapor duct yields an average temperature increase of approximately 1.5 ℃, which is the greatest reheating contribution among all the tested conditions and demonstrates the strengthened thermal coupling between the two stages.

Journal Pre-proofs

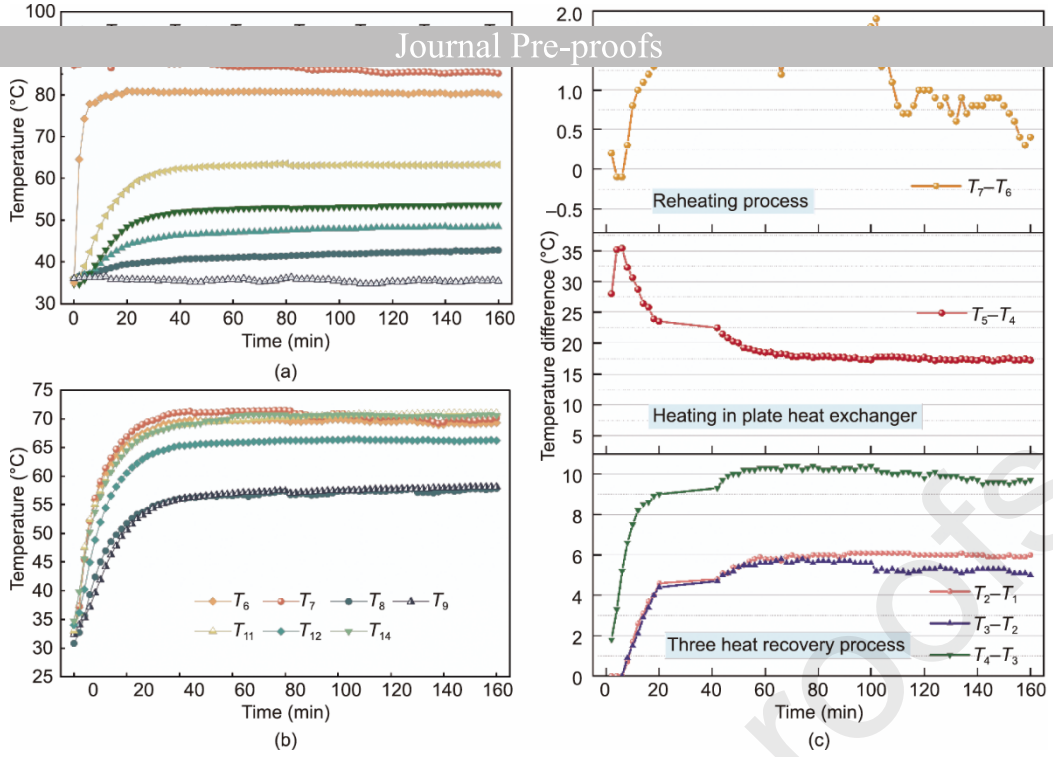

Fig. 6. Internal temperature distributions of the two-stage HDH desalination module at T_5 = 80℃; (a) Temperature evolution along the feed seawater preheating and heating pathway; (b) Temperature evolution in the high- and low-temperature HDH stages; (c) Temperature rises across the staged heat recovery, external heating, and reheating processes

A comparison of the four operating conditions reveals several consistent thermal behaviors within the HDH module. In each stage, the temperature of the condensed freshwater in the dehumidifier is slightly higher than that of the unevaporated feed seawater, which typically leaves the corresponding humidifier at less than 2 ℃. This close temperature correspondence suggests improved thermal matching between the humidification and dehumidification sections, thus mitigating heat transfer irreversibility associated with temperature mismatch during internal heat recovery. In all the cases, the spray temperature T_7 of the feed seawater entering the low-temperature stage exceeds the temperature T_6 of the unevaporated seawater leaving the high-temperature stage, and this temperature difference increases with increasing spray temperature T_5. This consistent temperature relationship confirms the positive temperature increase provided by vapor duct reheating before the second evaporation process.

The average temperature increases across the three internal heat recovery steps, external heating by the plate heat exchanger, and vapor duct feed seawater reheating under the tested spray temperature conditions are summarized in Fig. 7. As shown in Fig. 7(a), for each operating condition, the temperature rise of the first heat recovery step (T_2−T_1) consistently exceeds that of the second heat recovery step (T_3−T_2). This is mainly because the first step directly recovers sensible heat from the discharged brine to preheat the low-temperature feed seawater, whereas the second step is constrained by the lower condensation temperature in the low-temperature dehumidifier. In contrast, the temperature rise of the third heat recovery step (T_4−T_3) is markedly greater than those of the first and second steps, especially at higher spray temperatures. This reflects the higher heat recovery potential of the high-temperature dehumidifier, where vapor condensation and sensible cooling of the humid air release more heat to the feed seawater. This trend becomes more evident at higher spray temperatures. The data in Fig. 7(b) further indicate that the increase in (T_7−T_6) from 0.4 to 1.5 ℃ is associated with enhanced partial condensation and latent heat recovery in vapor duct at higher spray temperatures.

Journal Pre-proofs

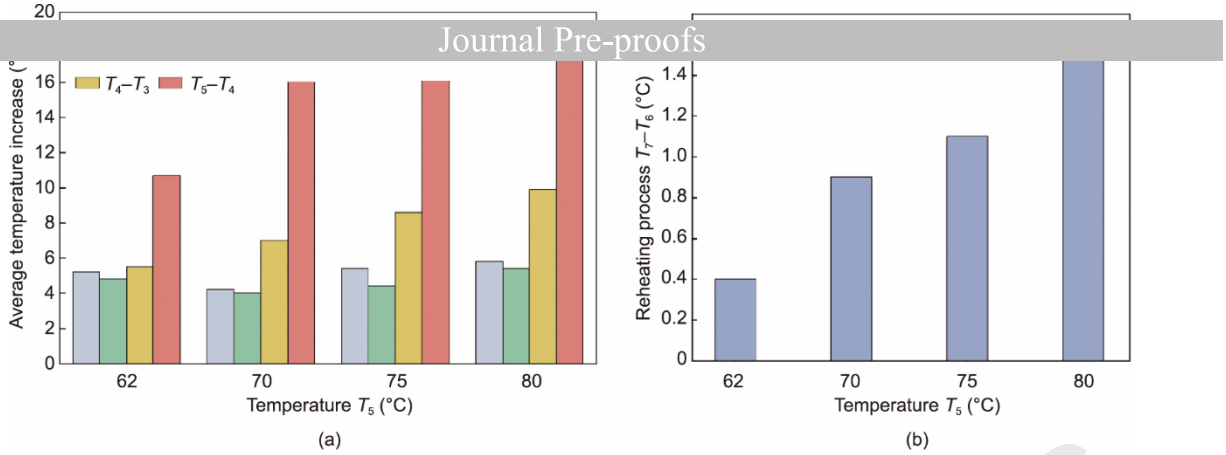

Fig. 7. Average temperature increases in staged heat recovery, plate heating, and reheating processes; (a) Temperature rises across the three heat recovery steps and the plate heat exchanger; (b) Temperature rise induced by vapor-duct reheating

3.2. Effects of spray temperature on freshwater production and GOR

On the basis of the theoretical model and experimental results, the effects of the high-temperature stage spray feed seawater temperature and vapor duct reheating process on the freshwater production rate and GOR of the system were evaluated.

The theoretical and experimental freshwater production rates are compared with those of vapor duct reheating in Fig. 8 (a). As shown in Fig. 8(a), the freshwater production rate increases rapidly as the seawater spray temperature in the high-temperature stage increases, with a particularly pronounced increase when the high-temperature stage of the spray seawater exceeds 70 ℃. With respect to the reheating process, the experimentally measured freshwater production rates at T_5 = 62, 70, 75 ℃, and 80 ℃ are 41.6, 54.9, 81.3, and 97.2 kg·h^{-1}, respectively. This nonlinear increase is associated with the temperature dependence of the air saturation-humidity ratio. At higher spray temperatures, the moisture carrying capacity of the air and the vapor pressure gradient increase substantially, thus intensifying evaporation in the humidifiers. Moreover, the higher temperature humid air promotes condensation in the dehumidifiers and provides more recoverable heat for the fine-grained heat recovery strategy. Together, these effects lead to significantly higher freshwater production at elevated spray temperatures of the feed seawater in the high-temperature stage.

The high-temperature stage consistently accounts for the majority of freshwater production. For instance, at T_5 = 75 ℃, the high and low-temperature stages produce 60.7 and 20.5 kg·h^{-1}, respectively, indicating that the high-temperature stage outperforms the low-temperature stage by nearly three times. This is due mainly to the greater difference in air water enthalpy, higher vapor pressure gradient, and stronger condensation heat release in the high-temperature stage, which together intensify the evaporation and condensation cycle.

A comparison between the experimental and theoretical results further reveals a temperature-dependent trend. When the spray temperature is less than 70 ℃, the theoretical model predicts slightly higher freshwater production than observed experimentally, whereas at spray temperatures above 70 ℃, the experimental production surpasses the predicted values. The deviation between the measured and calculated values remains within 7%–17%. The discrepancy between the theoretical and experimental results may be related to the assumptions, including ideal heat transfer conditions, uniform humid–air distribution, and simplified representation of heat loss and interstage heat exchange.

According to Fig. 8(b), a comparison with the reheating-enabled case clearly reveals that reheating provides a measurable performance advantage at the same heating temperature. For example, at T_5 = 80 ℃, the freshwater production rate increases from 88.2 (without the reheating process) to 97.2 kg·h^{-1} (with the reheating process). This increase occurs mainly because the reheating process increases vapor condensation in the high-temperature stage, as quantified by the additional heat recovery term $cm(T_7–T_6)$, and simultaneously increases the spray temperature entering the low-temperature stage, as shown in Fig. 7(b), thus strengthening the downstream humidification process. In contrast, at lower spray temperatures, such as T_5 = 62 ℃, the effect of the reheating process becomes negligible, and the freshwater production rates of the two cases show little difference. This is because the condensation potential at low-temperatures is small: the difference in temperature between the hot humid air and the unevaporated seawater ($T_7–T_6$) is minimal, and very little latent heat is left to recover. As a result, reheating provides almost no temperature increase for the feed seawater entering the low-temperature stage. In addition, the saturation humidity ratio and difference in vapor pressure are inherently low in this temperature range; thus, a small increase in the spray temperature has little effect on evaporation.

Fig. 8(c) shows that the GOR increases with T_5. This trend also results from the strong increase in the air humidity ratio at higher temperatures, which shifts a larger fraction of the spray-seawater sensible heat into evaporation rather than sensible convective exchange. As a consequence, latent heat utilization improves, leading to higher overall performance. At T_5 = 80 ℃, the GOR reaches 1.78 with the reheating process and 1.71 without it, which is higher than that of many conventional solar

driven two-stage HDH desalination systems

Journal Pre-proofs

3.3 Comparison with related HDH desalination systems

Fig. 8(d) [13,22,30,34,36,40 – 47] compares the pilot-scale solar powered two-stage HDH desalination system with reported representative HDH systems. Owing to limited internal heat recovery, the GOR of single-stage HDH systems is generally less than 0.9 [40, 41]. Compared with single-stage configurations, two-stage HDH systems introduce an additional humidification and dehumidification sections for recovering sensible and latent heat [42], thus improving the GOR. Among the reported two-stage HDH systems, a compact solar driven HDH system with a shared dehumidifier achieved a GOR of 0.84 and a freshwater production rate of 29.6 kg·h^{-1} [43], whereas a two-stage indirect solar dryer coupled HDH system reached a higher GOR of 1.38 but produced only 3.85 kg·h^{-1} of freshwater [44].

Although some two-stage systems report higher GOR values [45], these improvements are often achieved in small scale experimental setups rather than under pilot-scale operation. For example, a cylindrical Fresnel lens heated HDH system achieved a GOR of 2.1, but its maximum freshwater production rate was only 3.4 kg·h^{-1} [46], substantially lower than the 97.2 kg·h^{-1} obtained in this work. A three-stage HDH system was predicted to achieve a freshwater production rate of 151.2 kg·h^{-1} with a GOR of approximately 2.0 [47], but these results were based on thermodynamic modeling rather than experimental validation. In contrast, an experimentally tested four-stage HDH system produced about 63 kg·h^{-1} of freshwater with a GOR of around 1.4. In comparison, the present two-stage HDH system achieves a GOR of 1.78 and a freshwater production rate of 97.2 kg·h^{-1} under solar driven pilot-scale operation. This comparison indicates that the fine-grained heat recovery strategy can effectively increase heat utilization and maintain high freshwater production in a two-stage configuration, avoiding the additional structural complexity required by multi-stage HDH systems.

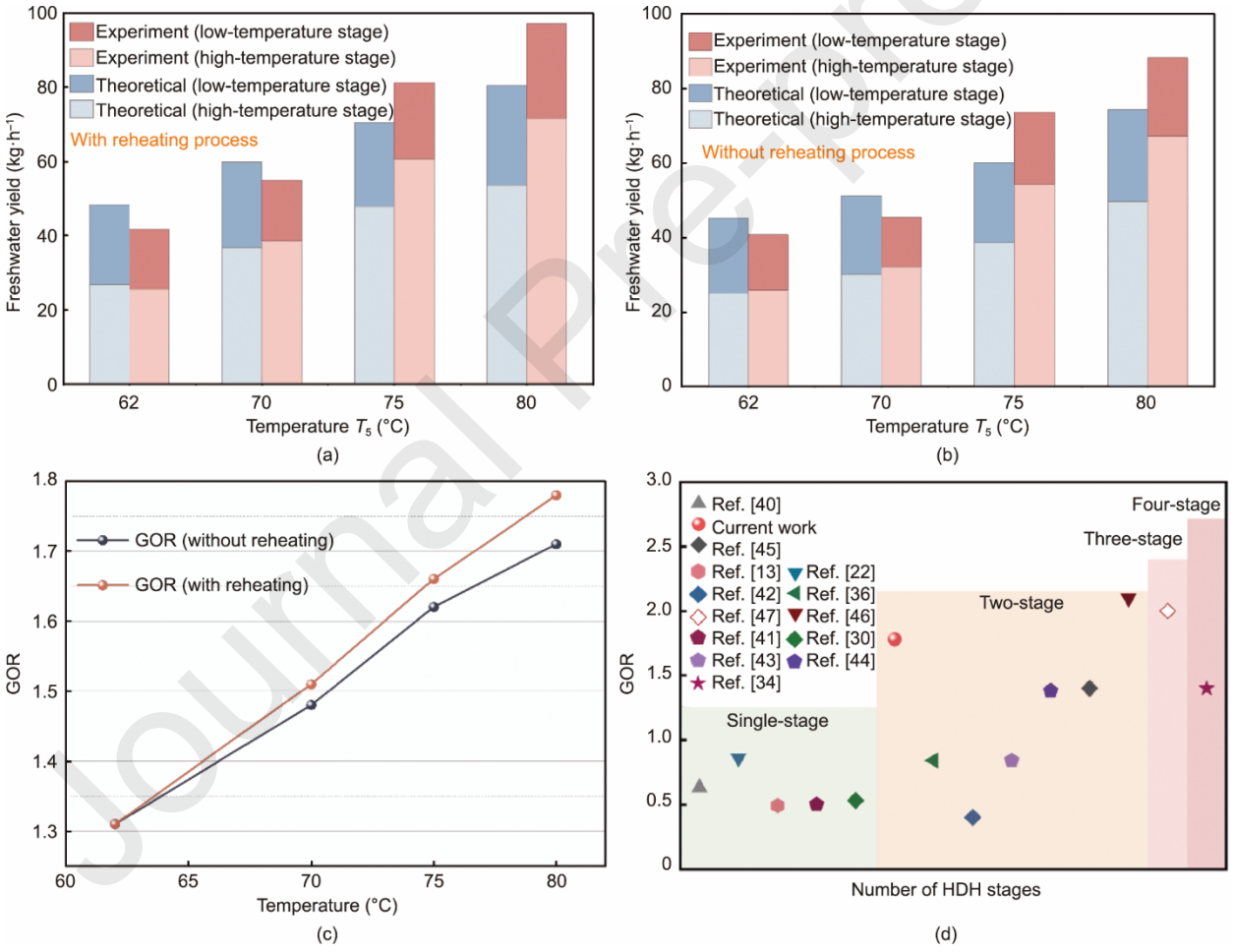

Fig. 8 Effects of the high-temperature-stage spray temperature and vapor-duct reheating on freshwater production and GOR; (a) Theoretical and experimental freshwater production rates with vapor-duct reheating; Theoretical and experimental freshwater production rates without vapor-duct reheating; (c) GOR with and without vapor-duct reheating; (d) Comparison of GOR with representative HDH desalination systems with different numbers of stages

3.4 Performance under fluctuating solar irradiance conditions

Journal Pre-proofs

After its performance under different fixed spray temperatures of the feed seawater was characterized, dynamic tests were conducted to evaluate the freshwater yield and GOR of the pilot-scale HDH system under fluctuating solar irradiance conditions. During the experiment, the HDH desalination system was automatically switched on when the solar storage tank temperature reached 80 ℃ and shut down when it fell to 55 ℃. A full-day experiment was conducted from 08:00 to 20:00, and the results are presented in Fig. 9.

Fig. 9(a) illustrates that from 08:00 to 11:00, as the solar irradiance steadily increased, the temperature of the solar storage tank increased from 30 to about 87 ℃. During this period, the tank temperature reached 55 ℃ at around 10:10, triggering the start-up of the HDH desalination system. By approximately 10:30, continuous freshwater production was established. From 11:00 to 16:00, the solar irradiance fluctuated, and the heat exchange between the solar storage tank and the HDH desalination module remained quasi-steady, with the water temperature inside the tank remaining above 85 ℃. During this period, the cumulative freshwater production increased almost linearly. As the solar irradiance gradually decreased after 16:00, the water temperature inside the tank began to decrease. Although the vacuum tube solar collector array could no longer operate effectively after 18:00, as sunlight was no longer available, the solar storage tank retained sufficient heat to sustain HDH operation until after 20:00, when the tank temperature dropped below 55 ℃.

During the entire test period, the total freshwater production reached 860 kg, as shown in Fig. 9 (b). In addition, the electrical conductivity of the produced water was measured to be 9 $mS \cdot m^{-1}$, corresponding to an estimated total dissolved solids (TDS) concentration on the order of tens of milligram per liter, which is far below the typical drinking-water guideline of about 500 $mg \cdot L^{-1}$. This finding indicates that the produced freshwater had low salinity and was broadly compatible with potable water requirements.

The GOR reaches 0.91 when the total incident solar energy, which is calculated as the product of solar irradiance, exposure time, and collector area, is taken as the system's thermal input. However, when the thermal input is defined more narrowly as the actual heat transferred from the solar collector loop to the desalination module, the calculated GOR reaches 1.8. This difference arises from the finite thermal efficiency of the solar collectors and the associated heat losses in the solar collectors, piping, storage tank, and other components. This GOR is greater than that of conventional two-stage HDH systems, demonstrating the effectiveness of the fine-grained heat recovery strategy.

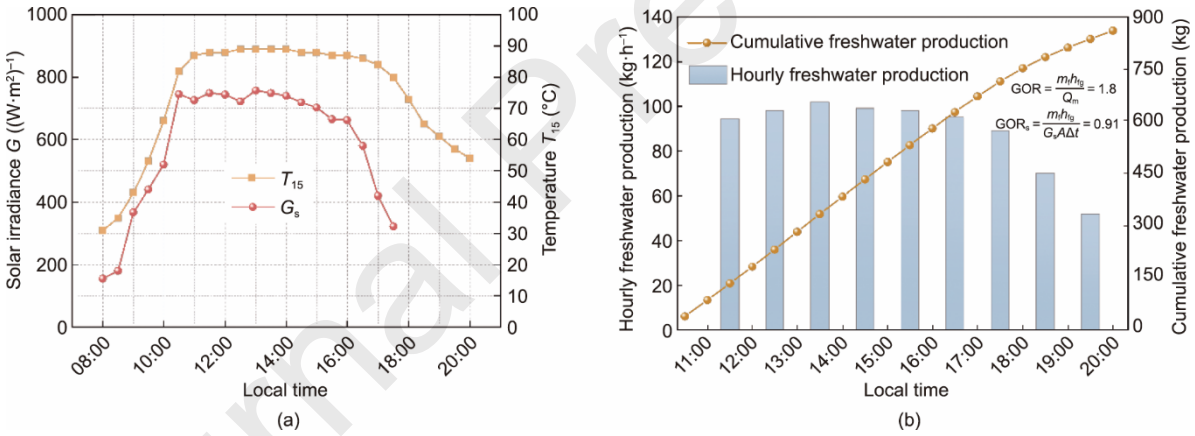

Fig. 9. Freshwater yield and GOR of the HDH under fluctuating solar irradiance conditions; (a) Temporal variations in solar irradiance and solar hot-water-tank temperature; (b) Hourly and cumulative freshwater production during full-day solar-driven operation.

4. Conclusions and outlook

4.1. Conclusions

Humidification–dehumidification (HDH) desalination is well suited for decentralized small and medium scale applications using low-temperature or solar thermal resources. Its practical performance, however, is constrained by inefficient internal heat recovery and insufficient utilization of condensation latent heat. To overcome these limitations, this paper proposes a fine–grained heat recovery strategy, which is accomplished by routing feed seawater through multiple heat recovery stages and using dual condensation to harvest latent heat from high-temperature humid air. A pilot-scale two-stage HDH desalination system powered by a 120 m^2 solar vacuum tube collector array was designed. Experiments at different spray temperatures, with and without reheating, and during full-day outdoor operation under fluctuating solar irradiance were conducted to evaluate its performance. The main conclusions are summarized as follows:

Freshwater production increases with increasing temperature in the high-temperature stage of the spray feed seawater temperature T_5. As T_5 increases from 62 to 80 ℃, freshwater production increases from 41.6 to 97.2 $kg \cdot h^{-1}$, and the GOR

increases from about 0.9 to 1.8, with a significant increase above ~70 °C because of the nonlinear increase in air humidity with

Journal Pre-proofs

Under all the conditions, the first heat recovery step provides a slightly greater temperature increases (T_2-T_1) than does the second step (T_3-T_2), typically approximately 4–6 °C versus 4–5 °C, whereas the third step in the high-temperature stage yields the greatest increase (T_4-T_3), reaching approximately 5.5–9.9 °C. This confirms that latent heat is most effectively recovered at a higher temperature level and that the fine–grained heat recovery network is effective.

The reheating process (T_7-T_6) can effectively improve HDH desalination performance at higher operating temperatures but has little effect at lower operating temperatures. At T_5 = 80 °C, the reheating process increases the freshwater production from 88.2 to 97.2 kg·h^{-1} and increases the GOR from 1.71 to 1.78, whereas at T_5 = 62 °C the differences in both freshwater production and the GOR between the two cases are small because of the limited recoverable latent heat.

A full-day experiment under fluctuating solar irradiance conditions revealed that the total freshwater production reached 860 kg, with a GOR of 1.8 when calculated on the heat delivered to the desalination module and 0.91 when calculated on the basis of the incident solar energy.

4.2. Outlook for practical implementation

Despite the enhanced performance demonstrated in this work, several limitations should be further addressed before practical application. The present study experimentally verified the proposed fine-grained heat recovery strategy under different spray temperatures and a full-day outdoor operation condition. However, its long-term stability under seasonal solar variation and continuous operation remains to be clarified. In particular, scaling and salt deposition on the packing materials, liquid distributors, and heat recovery coils may deteriorate the liquid distribution, increase the thermal resistance, increase the pressure drop, and gradually weaken the staged heat recovery effect. Therefore, future studies should conduct long-term pilot-scale tests with systematic monitoring of fouling behavior, pressure drop evolution, heat transfer degradation, brine discharge characteristics, and produced freshwater quality.

From a thermodynamic perspective, the key challenge is not only increasing the number of HDH stages, but also maintaining effective heat and mass transfer matching under fluctuating solar radiation and off-design operation. Adaptive regulation of the feed seawater flow rate, freshwater circulation rate, and air flow rate should be developed to preserve favorable temperature, humidity, and enthalpy profiles during both stages. In addition, an exergy analysis, a techno-economic assessment, and a life cycle evaluation are needed to quantify the practical benefits and environmental implications of the proposed configuration.

Acknowledgment

This work is supported by the National Key Research and Development Program of China (2025YFE0118800), the National Natural Science Foundation of China (NSFC; 52406215, 52476173, and U24A6007), and the Beijing Natural Science Foundation (L259010).

Data availability statement

The data that support the findings of this study are available from the corresponding author upon reasonable request.

Declaration of interest statement

The authors declare that they have no known competing financial interests or personal relationships that could have appeared to influence the work reported in this paper.

References

[1] Grafton RQ, Fanaian S, Horne J, Katic P, Nguyen NM, Ringler C, et al. Rethinking responses to the world's water crises. Nat Sustain 2025;8(1):11–21.

[2] Chang Z, Yang J, Chu Y, Hou J, Su Y. Energy, exergy and economic analysis of a novel immersion tapered solar still for combination with solar concentrator. Desalination 2025;601:118560.

[3] Shabib A, Tatan B, Elbaz Y, Aly Hassan A, Hamouda MA, Maraqa MA. Advancements in reverse osmosis desalination: technology, environment, economy, and bibliometric insights. Desalination 2025;598:118413.

Journal Pre-proofs

[4] Taraemi AA, Shahsavar SW. A state-of-art overview of multi-stage flash desalination and water treatment: principles, challenges, and heat recovery in hybrid systems. Sol Energy 2023;266:112157.

[5] Zhang H, Chen H, Wei Q, Zhang Z, Fang M, Yang J, et al. Study on mechanical vapor compression regeneration performance and process optimization of MEA absorbent solution. Therm Sci Eng Prog 2025;66:104065.

[6] Zheng Y, Zhu Z, Liang S, Ma X. Concentrated solar supercritical water desalination and multi-effect distillation hybrid systems for efficient zero liquid discharge. Desalination 2025;609:118890.

[7] Ghazy M, Zayed ME, Rehman S, Irshad K, Ibrahim EMM, Mohamed ASA, et al. Dynamic numerical modeling and performance assessment of a hybrid photovoltaic thermal collector adsorption desalination system for sustainable water–energy nexus. Sol Energy 2025;292:113441.

[8] Ben Khedher N, Mehryan SAM, Ahmed Alashaari GA, Alshehery S, Boujelbene M, Mahariq I. Enhancing solar desalination efficiency through integrated parabolic trough solar collector, porous media, and phase change material: a case study using Middle East weather data. Appl Therm Eng 2025;274:126672.

[9] Alnaimat F, Ziauddin M, Mathew B. A review of recent advances in humidification and dehumidification desalination technologies using solar energy. Desalination 2021;499:114860.

[10] Shalaby SM, Zayed ME, Hammad FA, Menesy AS, Elbar ARA. Recent advances in membrane distillation hybrids for energy-efficient process configurations: technology categorization, operational parameters identification, and energy recovery strategies. Process Saf Environ Prot 2024;190:817–38.

[11] El–Agouz SA, Abd Elbar AR, Aboghazala AM, Shahin M, Zakaria MY, Esmaeil KK, et al. Comprehensive parametric analysis, sizing, and performance evaluation of a tubular direct contact membrane desalination system driven by heat pipe-based solar collectors. Energy Convers Manage 2022;274:116437.

[12] Liao X, Lim YJ, Khayet M, Liao Y, Yao L, Zhao Y, et al. Applications of electrically conductive membranes in water treatment via membrane distillation: joule heating, membrane fouling/scaling/wetting mitigation and monitoring. Water Res 2023;244:120511.

[13] Alnaimat F, Ziauddin M, Mathew B. Humidification and dehumidification desalination utilizing ultrasonic atomization and direct solar energy harvesting. Desalination 2025;602:118636.

[14] Nabil I, Abdalla AM, Mansour TM, Shehata AI, Dawood MMK. Salinity impacts on humidification dehumidification (HDH) desalination systems: review. Environ Sci Pollut Res Int 2024;31(2):1907–25.

[15] Mokhtar RY, Shouman MA, Elmarghany MR, Hamed AM. Rethinking HDH desalination: a comprehensive review beyond energy towards, exergoeconomic, and renewable-based multigeneration evaluation. Desalination 2024;575:117286.

[16] Ghosh DP, Hassan M, Dennis SJ, Sharma D, Elhashimi-Khalifa MA, Abbasi B. Anti-fouling rotating polymer-based heat exchanger for zero liquid discharge humidification – dehumidification desalination. Water Res 2024;258:121749.

[17] Alsaman AS, Ghazy M, Ali ES, Askalany AA, Farid AM, Tawfik MHM. Solar–powered adsorption desalination utilizing composite silica gel with a humidification–dehumidification desalination system. Desalination 2024;582:117663.

[18] Santosh R, Yoo CH, Kim YD. Performance evaluation and optimization of humidification–dehumidification desalination system for low-grade waste heat energy applications. Desalination 2022;526:115516.

Journal Pre-proofs

[19] Abdelmageed MM, Zayed ME, Li Y, Zhao J, Rehman S, Irshad K, et al. Performance assessment of hybrid adsorption/humidification dehumidification desalination cycle powered by dish/stirling concentrated solar power system for sustainable freshwater production maximization. Process Saf Environ Prot 2025;193:1094–113.

[20] Tiwari A, Kumar A. Humidification–dehumidification desalination system based novel solar water heater: an experimental study. J Therm Anal Calorim 2025;150(23):19463–80.

[21] Abdullah AS, Aljaghtham M, Kandeal AW, Sharshir SW. Techno-economic investigation of an entirely solar-powered hybrid HDH/RO desalination plant for moderate water demand under various operating conditions. Results Eng 2024;24:103200.

[22] Mohamed ASA, Shahdy AG, Salem Ahmed M. Investigation on solar humidification dehumidification water desalination system using a closed-air cycle. Appl Therm Eng 2021;188:116621.

[23] Rahimi-Ahar Z, Hatamipour MS, Ahar LR. Air humidification–dehumidification process for desalination: a review. Pror Energy Combust Sci 2020;80:100850.

[24] Shaikh JS, Ismail S. A review on recent technological advancements in humidification dehumidification (HDH) desalination. J Environ Chem Eng 2022;10(6):108890.

[25] Wang Y, Ma X, Ouyang Z, Liang S. Comprehensive analysis of forced convection heat transfer enhanced by metal foam with pore density gradient structure. Sol Energy Mater Sol Cells 2025;285:113549.

[26] Wang Y, Sun X, Li L, Kang H, Shen L, Mao M, et al. Vibration-induced heat transfer enhancement in additively manufactured Kelvin metal foam. Appl Therm Eng 2025;274:126767.

[27] Thanaiah K, Gumtapure V, Mitiku Tadesse G. Experimental analysis on humidification–dehumidification desalination system using different packing materials with baffle plates. Therm Sci Eng Prog 2021;22:100831.

[28] Abedi M, Tan X, Saha P, Klausner JF, Bénard A. Design of a solar air heater for a direct-contact packed-bed humidification–dehumidification desalination system. Appl Therm Eng 2024;244:122700.

[29] Raj PR, Jayakumar JS, Ajith Kumar R. On the selection of humidification dehumidification desalination system cycle for high productivity, low energy consumption and low capital cost. Desalination 2024;586:117876.

[30] Liang S, Ma X, Zhang N, Zheng H. Effectiveness of a built-in air duct desalination machine with absorption process. Appl Therm Eng 2021;189:116708.

[31] Wang B, Shen J, Wei W, Jiang L, Chen Y. Evaluation of two-stage humidification–dehumidification desalination systems operated by a modified heat pump. Appl Therm Eng 2024;247:123041.

[32] Shamet O, Lawal DU, Alawad SM, Antar M, Zubair SM, Mansir IB, et al. Multi-stage humidification–dehumidification system integrated with a crystallizer for zero liquid discharge of desalination brine. Energy Convers Manage 2024;307:118340.

[33] Zamen M, Soufari SM, Vahdat SA, Amidpour M, Zeinali MA, Izanloo H, et al. Experimental investigation of a two-stage solar humidification–dehumidification desalination process. Desalination 2014;332(1):1–6.

[34] Zhao Y, Zheng H, Liang S, Zhang N, Ma X. Experimental research on four-stage cross flow humidification dehumidification (HDH) solar desalination system with direct contact dehumidifiers. Desalination 2019;467:147–57.

Journal Pre-proofs

[35] Zhao Z, Zheng H, Ma X, Liang S. Toward efficient thermal desalination via alternate vertical array flow of binary liquids. Appl Therm Eng 2025;265:125550.

[36] Yang J, Zheng H, Ma X, Liang S, Zhu Z. Experimental study on a compact solar driven two-stage humidification–dehumidification desalination system with shared dehumidifier. Appl Therm Eng 2024;249:123423.

[37] Nabil I, Dawood MMK, Mansour TM, Shehata AI, Abdalla AM. Improved productivity of seawater desalination systems through humidification–dehumidification process integrated with renewable and fogging technologies in a lowest cost. Appl Water Sci 2025;15(6):115.

[38] Chehayeb KM, Narayan GP, Zubair SM, Lienhard JH. Thermodynamic balancing of a fixed-size two-stage humidification dehumidification desalination system. Desalination 2015;369:125–39.

[39] Bihani R, Tan X, Saha P, Abedi M, Klausner J, Benard A. Modeling and validation of heat and mass transfer in a direct contact packed bed crossflow humidifier. Appl Therm Eng 2025;268:125961.

[40] Hatab SI, Abdel-Sayed AH, Mansour AS, Mubarak AK. Experimental study of productivity enhancement in a humidification – dehumidification desalination system through various packing materials and configurations. Sci Rep 2025;15(1):39547.

[41] Srithar K, Rajaseenivasan T. Performance analysis on a solar bubble column humidification dehumidification desalination system. Process Saf Environ Prot 2017;105:41–50.

[42] Antar MA, Khan MA, Faizan M, Khalifa AEJWS. Experimental study on optimum performance of two-stage air-heated bubble-column humidification–dehumidification system. 2023 Water SA;49(4):37486.

[43] Soomro SH, Ullah A, Soomro MI, Zulfiqar M. Performance evaluation of a two-stage humidification–dehumidification desalination process. Heat Transf 2026;55(3):1399–419.

[44] Kabeel AE, Abdelgaied M. Experimental evaluation of a two-stage indirect solar dryer with reheating coupled with HDH desalination system for remote areas. Desalination 2018;425:22–9.

[45] Faizan M, Toor Z, Antar MA. Optimization of two-stage modified air heated HDH desalination systems. Arab J Sci Eng 2022;47(12):16451–73.

[46] Wu G, Zheng H, Ma X, Kutlu C, Su Y. Experimental investigation of a multi-stage humidification–dehumidification desalination system heated directly by a cylindrical Fresnel lens solar concentrator. Energy Convers Manage 2017;143:241–51.

[47] Khass TM, Mohammed RH, Qasem NAA, Zubair SM. Different configurations of humidification–dehumidification desalination systems: thermal and economic assessment. Energy Convers Manage 2022;258:115470.

Declaration of interests

☒ The authors declare that they have no known competing financial interests or personal relationships that could have appeared to influence the work reported in this paper.

Journal Pre-proofs

☐The authors declare the following financial interests/personal relationships which may be considered as potential competing interests:

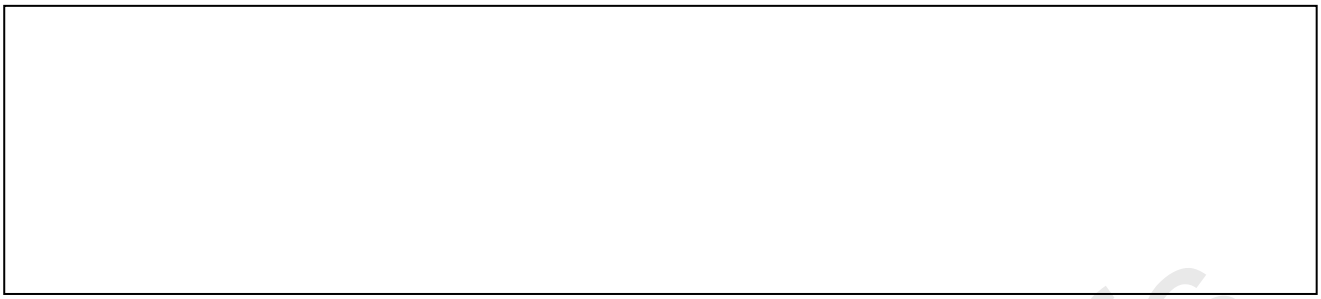

Journal Pre-proofs